Robust Continuous Wheel Slip Control With Reference Adaptation: Application to the Brake System With Decoupled Architecture

Dzmitry Savitski, *Member, IEEE*, Dmitrij Schleinin, Valentin Ivanov, *Senior Member, IEEE*, and Klaus Augsburg

***Abstract*—Modern and coming generations of electric and automated vehicles are characterized by higher requirements to robust and fault-tolerant operation of chassis systems independently from driving situations and road conditions. In this regard, this paper introduces an adaptive continuous wheel slip control (WSC) developed for the sport utility vehicle equipped with a high-dynamic decoupled electrohydraulic brake system. The system architecture, mathematical formulation of the WSC and state estimator as well as the experimental WSC validation is described in this paper. The focus is given on three continuous WSC strategies based on proportional integral (PI), sliding-mode PI and integral-sliding-mode control techniques. The proposed WSC also includes the state and parameter estimator for the adaptation of the reference wheel slip depending on current road conditions and using the standard on-board vehicle sensors and extremum-seeking algorithm. Adaptability and robustness of all WSC configurations were confirmed by the road experiments performed on low- and high-μ surfaces with mandatory condition of the same controls adjustments for all test cases. Tests show an enhancement of the vehicle safety and ride quality, compared to the vehicle with the rule-based WSC control.**

***Index Terms*—Adaptive control, sliding mode control (SMC), vehicle dynamics, vehicle safety, wheel slip control (WSC).**

I. Introduction

THE function of the wheel slip control (WSC) belongs to almost each class of driving safety tools as antilock braking, traction control, and vehicle stability control systems. In the most cases, industrial solutions for the WSC in the passenger cars use rule-based multiphase modulation of the wheel torque through hydraulic brake actuators. Such an approach demonstrated sufficient functionality for conventional vehicles to fulfil requirements of current regulations in driving safety. However, latest trends in vehicle electrification and automatization rise a question about revisiting of the WSC design that can be argued as follows.

As for electric vehicles (EV), the WSC functions can be efficiently realized with individual in-wheel or on-board motors [1], [2]. Recent studies show that electric motors not only allow better tracking of the target wheel slip but also provide more robust operation by coping with critical driving situations such as driving on split-road surface [3]. But strict legislative regulations and functional limitations for mass-production vehicles still require joint operation of electric motors and traditional chassis systems. The WSC in a braking mode should be realized in this regard with the brake blending with electric motors and friction brakes as actuators. As a consequence, it is required to have the friction brake system with the system response and system bandwidth comparable with electric motors.

Another problem of the WSC is recently emerged with the development of automated driving technologies [4], [5]. Coming generations of autonomous vehicles, especially on automation level 4–5 in accordance with SAE J3016 standard, should provide new driving comfort conditions considering limited awareness of the driver/passenger about an actual driving situation. In particular cases of the braking with the WSC activation, it means that the deterioration of the driving comfort caused by oscillatory jerk dynamics of the vehicle has to be minimized. However, it is very difficult to achieve this target by the conventional rule-based WSC with relay actuators of hydraulic brake systems.

Summarizing, the described problems of the WSC put demand on new brake actuators and appropriate control methods providing more sophisticated solutions to guarantee systems' integrity and fault-tolerant operation independently from driving situations and road conditions. In this regard, more attention in recent studies and industrial developments for the WSC is being paid to decoupled electro-hydraulic brake (DEHB) systems as actuating part. For EVs, the DEHB system architecture ensures the full braking functionality and fulfils

Manuscript received January 14, 2018; revised February 21, 2018; accepted March 12, 2018. Date of publication April 3, 2018; date of current version September 4, 2018. This work was supported in part by the Thuringian Center for Innovation in Mobilität and excellence center VISTA4F funded by the Federal State of Thuringia, Germany, under the Grant TUI-I-01-14 and in part by the European Union's Horizon 2020 research and innovation programme under the Marie Skłodowska-Curie Grant 645736. Paper no. TII-18-0114. *(Corresponding author: Dzmitry Savitski.)*

The authors are with the Automotive Engineering Group, Department of Mechanical Engineering, Technische Universität Ilmenau, 98693 Ilmenau, Germany (e-mail: dzmitry.savitski@tu-ilmenau.de; dmitrij.schleinin@tu-ilmenau.de; valentin.ivanov@tu-ilmenau.de; klaus.augsburg@tu-ilmenau.de).

Color versions of one or more of the figures in this paper are available online at http://ieeexplore.ieee.org.

Digital Object Identifier 10.1109/TII.2018.2817588

fail-safe requirements for serial production vehicles. For automated vehicles, the DEHB allows continuous control on the wheel torque that can potentially reduce the vehicle jerk oscillations at the braking. However, nowadays, there are no well-established control approaches to be applied to the WSC with the DEHB.

The WSC system typically consists of two main components: the slip controller and the reference wheel slip generator. The first part concerns the choice of appropriate controller architecture and design, while the latter relates to the state estimation problem.

Most of known studies in the WSC propose switching control logic methods, which are also traditionally being used in industrial antilock braking systems. For example, [6] demonstrates a solution based on nonlinear state feedback, which provides a robust system operation. In [7], the control is realized with the fuzzy logic with a reference slip estimation through the artificial neural network. In general, the switching control logic for the WSC uses predominantly the rule-based algorithms, where the control process consists in cyclic alternation of phases for the increase, decrease, and holding of the wheel torque depending on selected control thresholds by the wheel slip and acceleration. During several decades, there were no alternatives to such an approach due to a limited bandwidth and time response of the traditional hydraulic systems. However, from the beginning of 2000s, emergence of decoupled brake systems made possible implementation of continuous WSC algorithms with positive impact on the vehicle safety and ride quality.

The continuous control system can be potentially realized with many approaches, starting from well-known proportional-integral differential (PID) algorithms up to complex hybrid control methods. Considering typical WSC requirements in terms of real-time applicability and robustness to maneuver-/road-related uncertainties, it is difficult to select *a priori* a more suitable control technique. For example, the continuous WSC for EVs with electric motors as actuators has been experimentally investigated for proportional-integral (PI) algorithms [8], [9]. However, the robustness of the PI-based control for the DEHB is not well studied. Otherwise, among possible designs for the continuous WSC, the sliding mode control (SMC) can be considered as another suitable approach. One of the first SMC solutions for the WSC was proposed in [10] including the extremum seeking algorithm. In [11], the second-order sliding mode is utilized together with the estimation of tire–road friction based on the first-order sliding mode observer. The integral-type SMC with a state-dependent Riccatti equation as the nominal controller is discussed in [12] considering the WSC system reliability and actuator faults. The authors in [13] used the SMC with conditional integrators to suppress the chattering effect. The attenuation of the chattering caused by the the SMC was also addressed in [14] through offline optimization of controller gains. In [15], several SMC sliding surfaces for the WSC in a two-wheeled vehicle were analyzed in terms of robustness to uncertainties related to the tire–road interaction. Handling of such uncertainties is also addressed in [16], where the Grey system modeling approach was applied to the SMC. This approach achieved sufficient reduction of wheel slip oscillations even in cases of significant road friction variation. However, the most of analyzed research studies about the SMC in the WSC are limited by the lack of experimental validation, and in majority of cases, the reference wheel slip is considered as the constant value.

The latest mentioned aspect can be examined as one of the most critical parts of published studies about the WSC. Independently from the selected variant of the control technique, the WSC should provide reliable generation of the reference wheel slip ratio and its adaption to driving conditions. But only few published studies are known in this area. In particular, [17] proposed the reference slip estimation using the bootstrap Rao–Blackwellized particle filter based on the signals from the wheel speed sensors, accelerometer, and GPS. Estimation of the reference slip is also discussed and validated in simulation in [18], where wheel slip dynamics is handled as the second-order system based on the LuGre friction model. Feedback linearizing control is given in [19], where the optimal wheel slip area is determined by the extremum seeking algorithm based on the online optimization method, where the uncertain plant with unknown parameters is considered. However, as it can be concluded from the analysis of published research studies, robust and real-time capable methods of the reference wheel slip estimation are mainly based on the polynomial fitting algorithms. As it was demonstrated in [20]–[22], this method allows determination of extremum position using the conventional on-board vehicle sensors and applying methods requiring reasonable computational resources. However, there is limited information in relevant publications about the integration of the slip target adaptation mechanisms into the overall control architecture. In light of the described scope of problems, this study has the following objectives.

1) To analyze the main technical requirements to the DEHB in scope of the continuous WSC, modify the system (individual wheel torque control and accurate wheel speed measurements), and implement this on the vehicle demonstrator.
2) To establish the basis control algorithm of the WSC (PI) with a novel activation and deactivation mechanism (antiwindup part instead of sophisticated rule-based logic).
3) To establish the agile and robust continuous WSC [sliding-mode PI (SMPI) and integral sliding mode (ISM)], which can handle such uncertainties as road friction variation and vertical load distribution without their estimation.
4) To develop reference adaptation logic for providing the maximal braking force independently from the road conditions.
5) To investigate the functionality of the continuous WSC in terms of safety (braking distance) and ride quality (longitudinal vehicle jerk), control performance (deviation of the actual wheel slip from reference), adaptability (capability of the algorithm to identify the appropriate wheel slip reference), and robustness (sensitivity to road friction changes and variation of main characteristics for several repetitions) for the vehicle with the DEHB system as the WSC actuator.

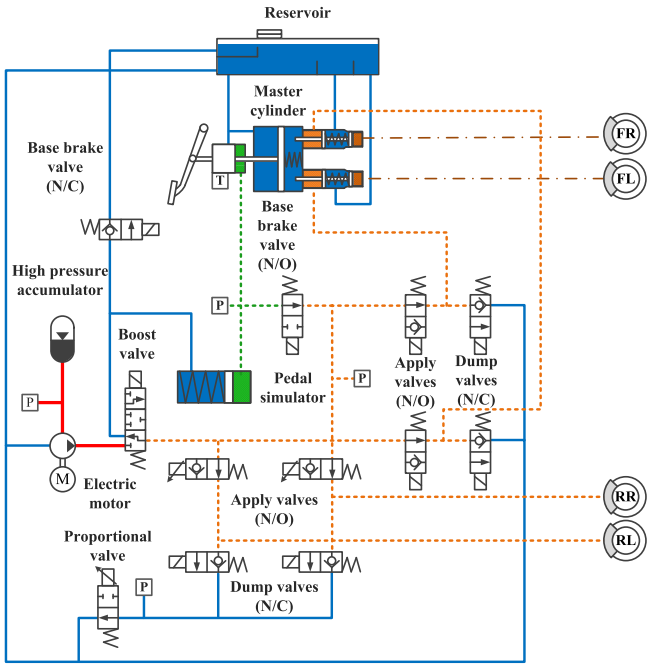

Fig. 1. Hydraulic scheme of the SCB brake system.

6) To compare experimentally performance of developed continuous control approaches for the WSC (PI, SMPI, and ISM) methods with the aim to select an appropriate candidate for the DEHB-based WSC as compared with switching rule-based control logic.

Following these objectives, this paper will introduce the DEHB integration and the control for the sport utility vehicle (SUV) with the focus on the fail-safe operation and adaptive WSC strategy, which is robust to the road uncertainties. The DEHB architecture and evaluation of the system performance is described in Section II. Section III introduces the wheel slip controller and applied control methods. As the basic solution, the PI control with an implemented deactivation function is proposed. To improve robustness of this one, an SMPI control with a double-integral sliding surface is further introduced. To suppress chattering effect coming from the SMPI, the third control strategy is represented by the ISM control. Section IV describes the developed state and parameter estimator and discusses the procedure of the reference slip estimation and adaptation. Experimental results from road tests are given in Section V showing benefits of the developed WSC types over switching rule-based (RB) control logic used in serial production vehicles.

II. Specifications of the Decoupled Brake System

The WSC in this study uses the DEHB system based on the slip control boost (SCB) technology developed by the ZF TRW Automotive [23] for EVs and HEVs to provide brake blending functions as well as to fulfill legislatively obligated fail-safe operation. Compared to the serial production system, internal control logic was modified in this study to allow an individual brake torque control at each wheel.

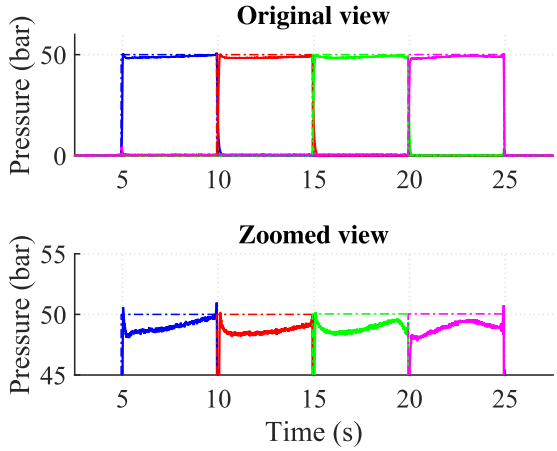

Fig. 2. Pressure step response. An HPA allows quicker pressure buildup compared to the conventional EHB systems.

As it is shown in Fig. 1, the pedal travel sensors of the unit and the pressure sensor on the base-brake valve allow estimating the braking demand requested by a driver. This information is postprocessed in the vehicle control unit (VCU) and corresponding brake pressure demands are calculated. These values are further transmitted to the electrohydraulic control unit (EHCU), where feedback pressure control is realized internally. It is based on the pressure measurements in hydraulic circuits of the EHCU and indirect estimation of four brake caliper pressures $\hat{P}_{\text{cal}}^{ij}$ (herein and after $i = \{F; R\}$ and $j = \{L; R\}$ correspond to the wheel position). The presence of the pressure $\hat{P}_{\text{cal}}^{ij}$ allows more precise estimation of vehicle states, as reported in [24]. The force feedback on the brake pedal is performed through the pedal simulator generating appropriate pressure in the primary circuit of the master cylinder. As a benefit, the presented DEHB design shows lower variation of the pedal force compared to the conventional systems. Besides that, the system can maintain the desired brake pedal feel independently from the reference brake pressure, which is important point for the brake blending and automated braking functions. Such system architecture allows to omit the use of the brake booster that is of benefit in terms of system's compactness. The base brake valves are activated during the moderate braking. The boost valve proportionally controls the pressure from the high-pressure accumulator (HPA). The brake pressure on wheel calipers is continuously modulated in accordance with the internal control logic of the EHCU. During the WSC mode, four apply valves are activated in the case of the excessive wheel slip in order to isolate the boost valve from the wheel calipers. Then, both apply and dump valves are individually controlled and modulate the pressure for each wheel brake to reach the desired wheel slip.

Pressure in an HPA is observed by the sensor to keep its level at 180 bar. Compared to the conventional brake systems, this allows quicker buildup of the caliper pressure providing 85–200 ms shorter rise time during the step pressure request, Fig. 2. Besides that, utilization of the proportional valves instead of the traditional relay valves allows more precise pressure tracking during progressive pressure buildup or dump; see Fig. 3.

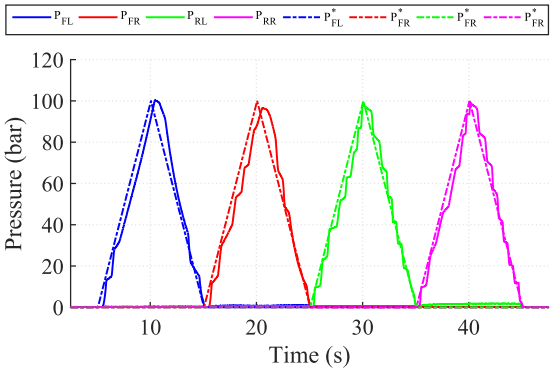

Fig. 3. Slowly increasing pressure ramp. Through utilized proportional valves, system can provide precise pressure tracking, which is complicated to achieve with only relay valves.

TABLE I
SCB BRAKE SYSTEM

Test	Evaluation metric	Wheel position FL	FR	RL	RR
Step response	Rise time (ms)	100	140	110	110
	Pressure RMSD[1] (bar)	0.5	0.8	0.4	0.4
Slow ramp increase	Pressure RMSD (bar)	2.4	2.5	1.9	1.8
	Gradient STD[2] (bar/s)	19.9	19.9	25.9	23.4
Slow ramp decrease	Pressure RMSD (bar)	1.9	1.9	1.1	1.1
	Gradient STD (bar/s)	19.5	19.8	25.9	25.9

[1] Root-mean-square deviation
[2] Standard deviation

Corresponding evaluation metrics of the introduced DEHB system are summarized in Table I.

Original wheel speed sensors are used to estimate the wheel slip. To avoid distortion of control functions of the VCU, these sensors are supplying information about the wheel speeds to the EHCU as well as to the VCU in parallel. This was done by electrical isolation of the signals between these two control devices by inclusion of developed electrical circuit. Information about the wheel speeds was used from the high-speed controller area network (CAN) frame with sampling time $t_s = 3$ ms. This allows a more agile WSC, as the wheel speeds information obtained through the on-board-diagnose port of the VCU has $t_s = 20$ ms. An infinite impulse response discrete filter was applied to the wheel speeds. After electrical decoupling, analogue sensors on the front wheels produced more noise than digital sensors on the rear. Therefore, the cutoff frequency for the front wheels is selected at 20 Hz, while cutoff of 30 Hz was used for the rear ones. Important to admit, that a higher sampling rate of the original signal allows obtaining more precise information about the wheel speeds (see Fig. 4), although the filter has a bandwidth of 30 Hz.

III. WSC

A. Control Description

In accordance with Fig. 5, the WSC functions are realized by generating reactive torque T_{react} and subtracting this from the individual wheel torque demands T_{dist}, which are based on the distribution of the base-brake torque T_{bb} between the wheels.

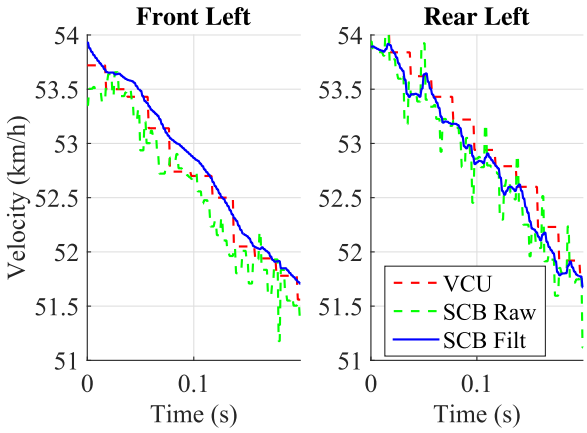

Fig. 4. Wheel speed sensors information obtained over the VCU and EHCU controllers. The applied decoupling scheme allows a higher sampling rate for all wheels and lower phase for the rear wheels.

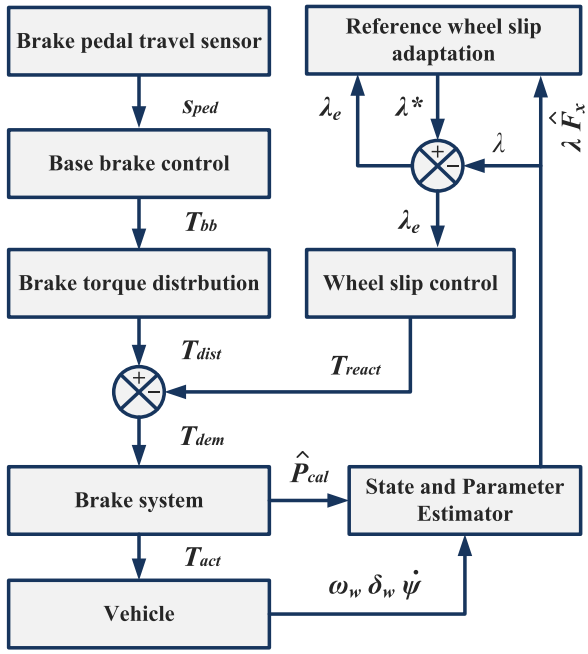

Fig. 5. Architecture of the proposed WSC.

The base-brake torque T_{bb} demand is calculated using the information about brake pedal travel s_{ped} obtained from the sensor measurements. Calculation of the actual wheel slip λ is based on the vehicle velocity $\hat{V}_x$ estimation, while the reference wheel slip λ^* is computed using obtained λ and estimated longitudinal wheel force $\hat{F}_x$. Further three methods (PI, SMPI, and ISM) applied for generating reactive torque T_{react} are explained.

B. Wheel Dynamics

For designing the WSC, a single corner model is used, which is described by the following system of equations neglecting transient tire dynamics:

$$\begin{cases} J_w \dot{\omega} = r_w F_x - T_b \\ m \dot{V}_x = -F_x = -F_z \mu(\lambda) \end{cases} \tag{1}$$

where V_x is the vehicle longitudinal velocity, ω is the angular wheel speed, m is the mass of quarter vehicle, J_w is the wheel inertia, r_w is the wheel radius, T_b is the braking torque, F_x is the longitudinal tire force, F_z is the vertical tire force, $\mu(\lambda)$ is the friction coefficient between tire and road, λ is the longitudinal wheel slip, and F_x is the tire longitudinal force.

For the braking mode, a positively defined wheel slip is represented as

$$\lambda = \frac{V_x - \omega r_w}{V_x}. \tag{2}$$

The wheel slip dynamics can be deduced from (1) and (2) as

$$\dot{\lambda} = -\frac{1}{V_x}\left(\frac{1}{m}(1-\lambda) + \frac{r_w^2}{J_w}\right) F_z \mu(\lambda) + \frac{r_w}{J_w V_x} T_b. \tag{3}$$

In the case $V_x \to 0$, loss of controllability is determined by infinitely fast system dynamics. Therefore, the WSC should be deactivated at relatively low values of the V_x.

Equation (3) can be reduced to

$$\dot{\lambda} = -\frac{1}{V_x}\frac{r_w^2}{J_w} F_z \mu(\lambda) + \frac{r_w}{J_w V_x} T_b, \text{as } \frac{1}{m}(1-\lambda) << \frac{r_w^2}{J_w}. \tag{4}$$

Following assumptions are done in the represented model [25].

1) Tire vertical load distribution and pitch dynamics are not explicitly presented, as the suspension dynamics are neglected and wheels are considered to be dynamically decoupled.
2) The relation between the longitudinal tire force and vertical load F_z is linear.
3) The tire transient dynamics is neglected.
4) The model represents straight-line braking cases in terms of modeling and linear analysis. For the braking in a turn simulations, the coefficient of friction should be handled as the function also of the camber angle and wheel slip angle.
5) The wheel radius is considered to be constant. In this particular case, it was found by laboratory tests that this type of tires produces miserable variation of the tire effective radius for corresponding range of the wheel loads. Therefore, the tire radius was measured experimentally and considered as the constant value for the purposes of control design.

Despite these assumption, this representation of the wheel dynamics provides the sufficient description of the system for the control design purposes as it is stated and confirmed by the corresponding analysis in [25]. Moreover, such effects as the load distribution induced by the longitudinal acceleration of the vehicle (F_z) and variation of the road friction ($\mu(\lambda)$) should be handled as the uncertainty in SMPI and ISM controls to avoid additional state estimation. In the next subsections, PI, SMPI, and ISM controls are introduced.

C. PI Control

A reactive torque T_{react} for the WSC is applied in cases, where the wheel slip λ becomes higher than the reference value λ^*. This situation means that wheel torque exceeds physical limits determined by the road friction, and further, increase of the wheel torque follows to the degradation of the braking force. To avoid that, the wheel slip λ should be kept at the reference λ^* value, which corresponds to the maximal braking force on the F_x-λ diagram. Therefore, the control for the positively defined wheel slip is based on the error derived as

$$\lambda_e = \begin{cases} \lambda - \lambda^*, & \text{if } \lambda > \lambda^* \\ 0, & \text{otherwise.} \end{cases} \tag{5}$$

Considering this control error formulation, the PI control law is proposed as

$$u_{pi} = K_p\left(\hat{V}_x\right)\left(\lambda_e + \frac{\int \lambda_e dt}{t_i\left(\hat{V}_x\right)}\right) - u_{pi}\frac{\int \lambda_{e,\text{lin}} dt}{t_a\left(\hat{V}_x\right)} \tag{6}$$

where K_p is the proportional gain, t_i is the tuning parameter related to the I-contribution, t_a is the tuning parameter of the antiwindup part. The control gain K_p and tuning parameters t_i and t_a are scheduled and represented as the function of estimated longitudinal vehicle velocity $\hat{V}_x$ to produce the consistent system response independently from V_x variation.

The antiwindup part reduces the WSC interaction in the linear area and progressively deactivates the WSC using following formulation of the error for the cases $\lambda < \lambda^*$:

$$\lambda_{e,\text{lin}} = \begin{cases} \lambda^* - \lambda, & \text{if } \lambda < \lambda^* \\ 0, & \text{otherwise.} \end{cases} \tag{7}$$

Inclusion of this component significantly reduces complexity of the WSC deactivation rules compared to known approaches. The PI method provides simple solution for the continuous WSC. However, this approach is very sensitive to the variation of the road conditions, i.e., oscillatory behavior of the wheel slip may occur, as a consequence. To resolve this issue, the SMPI control is further proposed.

D. SMPI Control

SMPI control with a double-integral sliding surface is developed for the WSC to improve the system robustness. In SMPI, the switching control guarantees that the system moves toward the sliding surface and provides better robustness, compared to the PI control. SMPI control effort includes two parts

$$u_{sm} = u_c + u_d \tag{8}$$

where u_c and u_d are the continuous and discontinuous parts.

The continuous part is considered as the PI control from (6). For the situations where $\lambda > \lambda^*$, the continuous part can be determined as

$$u_c = \frac{1}{B(x)} K_P\left(\lambda_e + \frac{1}{t_I}\int \lambda_e dt\right) \tag{9}$$

and the input matrix $B(x)$ is defined as

$$B(x) = \frac{1}{V_x}\frac{r_w}{J_w}. \tag{10}$$

The discontinuous control part is formulated as

$$u_d = \frac{1}{B(x)} K_{\text{sw}} \text{sign}(s) \tag{11}$$

where K_{sw} is the control gain and s is the sliding surface.

The double-integral sliding surface is defined as

$$s = \lambda_e + K_1 \int \lambda_e dt + K_2 \int \left(\int \lambda_e(\tau) dt \right) dt \tag{12}$$

where K_1 and K_2 are the positive constants.

Using (10), (4) can be rewritten as

$$\dot{\lambda} = -B(x) r_w F_z \mu(\lambda) + B(x)u + B(x) T_{w,\text{unc}} \tag{13}$$

where $T_{w,\text{unc}}$ is the wheel torque describing uncertainties.

As it can be seen in (4), tire–road friction coefficient should be observed. A rapid estimation of the friction coefficient is difficult and practically unreliable that can produce negative influence on the overall control performance. Therefore, to avoid negative influence of the estimation error, following components are considered as the uncertainty:

$$h(x) = -B(x) r_w F_z \mu(\lambda) + B(x) T_{w,\text{unc}} \tag{14}$$

where $|h(x)| < h_{\max}$.

Defining $K_1 = Kp$ and $K_2 = \frac{Kp}{t_i}$ and assuming slow variation of λ^*, i.e., $\dot{\lambda}^* = 0$, the following can be obtained

$$\dot{s} = \dot{\lambda}_e + K_p \lambda_e + \int \frac{K_p}{t_i} = h(x) - K_{\text{sw}} \text{sign}(s). \tag{15}$$

Defining the Lyapunov candidate as [26]

$$V = \frac{1}{2} s^2 \tag{16}$$

the system is asymptotically stable if

$$\dot{V} = \frac{1}{2} s\dot{s} = s(h(x) - K_{\text{sw}} \text{sign}(s_0)) < 0. \tag{17}$$

Therefore, the system is asymptotically stable for

$$K_{\text{sw}} > |h_{\max}|. \tag{18}$$

Selection of the control gain K_{sw} in the aforementioned equation is based on the simulation with the validated vehicle model and assessment of $|h_{\max}|$ values. Despite SMPI provides a robust solution for the WSC, this approach can suffer from the chattering, which is typical for this class of controls. To solve this issue, ISM control is further proposed.

E. ISM Control

For ISM control, the motion equation of the system in sliding mode is of the same order as the original system [27]. The ISM provides compensation and estimation of the perturbations with less chattering compared to the SMPI. In the common form, the wheel slip dynamics can be expressed as the system operating under uncertainties as

$$\dot{x} = f(x) + B(x)u + h(x), \text{where} |h(x)| < h_{\max}. \tag{19}$$

The ISM control effort consists of two contributions:

$$u_{\text{ism}} = u_c + u_d. \tag{20}$$

The PI controller is used as the continuous part. According to the typical sliding mode, the discontinuous part has following representation:

$$u_d = -K_{\text{ism}} \text{sign}(s) \tag{21}$$

where K_{ism} is the control gain of the discontinuous part.

To reduce chattering and provide smooth control action, the discontinuous control is filtered. A first-order linear filter should be tuned so that it does not distort the slow component of the switched action [26]

$$u_d = \dot{u}_d^{\text{filt}} \tau_{\text{sw}} + u_d^{\text{filt}}. \tag{22}$$

Time constant τ_{sw} should be selected so small that the linear filter does not deteriorate the slow component of the switching action.

The sliding surface consists of the two parts and defined as

$$s = s_0 + z \tag{23}$$

where z is the integral term, and $s_0 = \lambda - \lambda^*$ is the sliding variable as in the conventional sliding mode.

Subtracting derivative of the reference wheel slip from the left and right sides of (4) yields

$$\Delta\dot{\lambda} = \dot{\lambda} - \dot{\lambda}^* = -\dot{\lambda}^* - B(x) r_w F_z \mu(\lambda) + B(x)u + B(x) T_{w,\text{ unc}} \tag{24}$$

where the reference wheel slip λ^* is considered as the known variable, and $f(x) = \lambda^*$, the additional wheel torque $T_{w,\text{unc}}$ describes uncertainties. The uncertainty is defined as in the case of the SMPI control in (14).

Using previous equations, the auxiliary variable z equals to

$$\dot{z} = -\frac{\partial s_0}{\partial(\lambda - \lambda^*)}(-\dot{\lambda}^* + B(x)(u_{\text{ism}} - u_d)) = \dot{\lambda}^* - B(x)(u - u_d). \tag{25}$$

The time derivative of the Lyapunov function should be negative to guarantee the asymptotically stable system. Since

$$\begin{aligned} \dot{s} &= s_0 + z = \dot{\lambda} - \dot{\lambda}^* + \dot{\lambda}^* - B(x)(u - u_d) \\ &= h(x) + B(x)u_{\text{ism}} - B(x)(u_{\text{ism}} - u_d) = h(x) - u_d \\ &= h(x) + B(x)u_d = h(x) - B(x)K_{\text{ism}} \text{sign}(s) \end{aligned} \tag{26}$$

following inequality

$$\dot{V} = \frac{1}{2} s\dot{s} = s(h(x) - K_{\text{ism}} \text{sign}(s)) < 0 \tag{27}$$

is satisfied for

$$K_{\text{ism}} > \left| \frac{h_{\max}}{B(x)} \right|. \tag{28}$$

Similar to the SMPI control, K_{ism} is selected using simulation results with the experimentally validated vehicle model.

IV. Reference Wheel Slip Adaptation

Some of the required system states cannot be measured directly, or corresponding sensors are too expensive to be used in serial production vehicles. To resolve this issue, a state estimator with a modular architecture was designed using the signals from

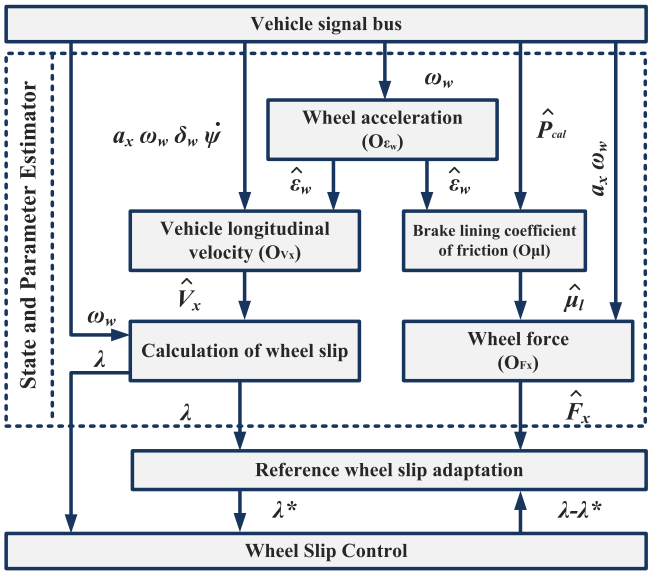

Fig. 6. State and parameter estimator.

the wheel speed sensors and inertial measurement unit (IMU). Modular approach in this case allows to avoid inclusion of nonlinear equations that provides benefits for observability analysis and tuning. The estimation architecture is given in Fig. 6. The velocity estimator O_{V_x} is based on the adaptive Kalman filter, where adaptation of covariance matrices requires the comparison of the wheel $\hat{\varepsilon}_w$ and vehicle a_x accelerations. a_x is used in the estimation procedure also to allow all four wheels to have the nonzero wheel slip during the WSC operation. This is not typical for serial production vehicles, where at least one of the wheels should provide information about the current vehicle velocity. The estimator of the brake lining coefficient of friction O_{μ_l} applies the recursive least-squares (RLS) method using wheel dynamics equations and the caliper pressure $\hat{P}^{ij}_{\text{cal}}$. This information is then applied in estimation of the individual tire forces O_{F_x}, where input torque from the system is corrected according to the variable value of μ_l. Estimator O_{F_x} uses knowledge about wheel dynamics and longitudinal dynamics of the vehicle. The calculated wheel slip and estimated forces are then routed to the reference wheel slip adaptation (RA) algorithm deriving F_x–λ characteristics of the tire. Experimental validation of the proposed state and parameter estimator is presented in Appendix A on Figs. 13, 14 and 15.

For the extremum seeking and definition of the reference wheel slip λ^*, the gradient of $\frac{\partial \hat{F}_x}{\partial \lambda}$ is identified by fitting the polynomial. Across several approaches, where functions of different complexity were used for this purpose [21], [28], solution with the linear function is selected

$$\hat{F}_x = C_1 + C_2\lambda \tag{29}$$

where C_1 and C_2 are coefficients of the polynomial.

The polynomial is fitted then to the collected set of force $\hat{F}$ and wheel slip λ during the predefined time period. These coefficients are estimated by solving the polynomial fitting task. Compared to the approaches, where nonlinear functions are fitted, this one requires a linear parameter estimation procedure using the RLS method

$$y = X^T\theta \tag{30}$$

where $y = \hat{F}_x$, $X = [1 \quad \lambda]^T$, and $\theta = [C_1 \quad C_2]^T$.

Algorithm 1: Seeking for the Optimal Reference Wheel Slip λ^*.

Require: Brake pedal travel s_{ped}, wheel slip $\lambda^{ij}_w(t)$, estimated wheel force $\hat{F}_x(t)$, estimated slope sign $\text{sign}(\nabla f) = \text{sign}\left(\frac{\partial \hat{F}_x}{\partial \lambda}\right)$.

Ensure: Reference wheel slip $\lambda^* \hat{=} \max\{F_x(\lambda)\}\ \forall \lambda \in [0,1]$.

Parameters: λ_{lim} is the minimal value of considered wheel slip, $\lambda_{e,\text{lim}}$ is the threshold of control error, K_λ is the adaptation ratio, n is the number of time samples during which gradient is calculated, and λ^{ij}_d is the desired wheel slip recognized as the optimal.

Initial value $\lambda^{*,ij} = \lambda_{\text{init}}$ corresponds to the higher values of the wheel slip to avoid fault interaction of the WSC.
Peak detection to activate the WSC:
if $s_{\text{ped}} > 1$ mm and $\lambda^{ij} > \lambda_{\text{lim}}$ and $\text{sgn}(\nabla f^{ij}_k) \neq \text{sgn}(\nabla f^{ij}_{k-1})$ **then**
    $\lambda^{*,ij}_k = \frac{1}{k-n}\sum_{i=k-n}^{k}\lambda^{ij}(i)$
    $\lambda^{ij}_{d,k} = \lambda^{*,ij}_k$
else
    $\lambda^{*,ij}_k = \lambda^{*,ij}_{k-1}$
end if
After WSC activation, $\lambda^{*,ij}$ is progressively adapted:
if $s_{\text{ped}} > 1$ mm and $\lambda > \lambda_{\text{lim}}$ and $\text{sgn}(\nabla f_k) \neq \text{sgn}(\nabla f_{k-1})$ & $|\lambda_k - \lambda^{*,ij}_k| < \lambda_{e,\text{lim}}$ **then**
    $\lambda^{ij}_{d,k} = \frac{1}{k-n}\sum_{i=k-n}^{k}\lambda^{ij}(i)$
    $\lambda^{*,ij}_k = \lambda^{*,ij}_{k-1} + K_\lambda\int_{t_{k-1}}^{t_k}\left(\lambda^{ij}_{d,k} - \lambda^{*,ij}_{k-1}\right)$
else
    $\lambda^{*,ij}_k = \lambda^{*,ij}_{k-1} + K_\lambda\int_{t_{k-1}}^{t_k}\left(\lambda^{ij}_{d,k} - \lambda^{*,ij}_{k-1}\right)$
end if
Apply $\lambda^{*,ij}$ to the WSC.

Information about y and X is collected during the predefined time Δt, and the length of these elements is $n = \frac{\Delta t}{t_s}$. The sign of the C_2 corresponds to the sign of the gradient $\frac{\partial \hat{F}}{\partial \lambda}$. As soon as the $\frac{\partial \hat{F}}{\partial \lambda}$ gradient is obtained, initial reference set point λ^*_{init} can be determined by taking the mean value of $\left[\lambda(t_1)\ \ldots\ \lambda(t_n)\right]$. In this form, rapid variation of the reference wheel slip can occur, which causes the oscillatory WSC behavior. Therefore, additional set of adaptation rules should be applied providing the reference slip value as slowly varying parameter and omitting its variation due to the high values of the control error. These rules are summarized in Procedure 1.

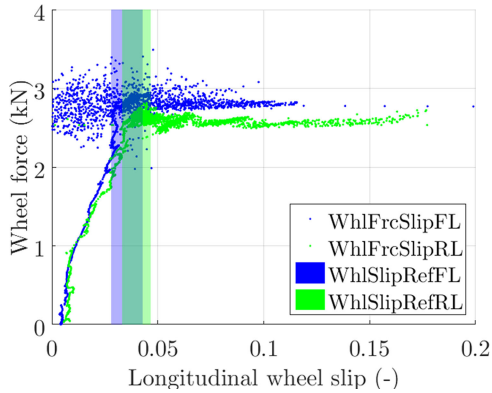

Fig. 7. Reference wheel slip adaptation during the WSC mode. Variation range of the reference wheel slip lies at the maximum of the estimated "tire force-wheel slip" diagram.

Fig. 8. Vehicle demonstrator on the low-μ road surface during testing in severe weather conditions. Represented road section is covered with the special friction layer, which is continuously wet with water sprinklers.

The experimental validation of the introduced reference adaptation logic on the low-μ road surface is represented in Fig. 7. Important to admit that this figure does not represent classical wheel slip thresholds but shows in which range the reference wheel slip has been varied. As it can be seen, during the braking, the reference wheel slip value remains so close to the peak value of the wheel force as possible.

V. Experimental Results

The SUV demonstrator equipped with a DEHB system and used in tests is shown in Fig. 8. Technical specifications of the vehicle are presented in Table III in Appendix B. The standard wheel speed sensors and IMU are used for the state and parameter estimation. For the state estimator validation, additional measurement systems were installed: dSPACE processor board DS1007 with digital input/output, CAN and multichannel A/D boards; brake pressure sensors; brakes temperature sensors; Kistler wheel force sensor RoaDyn S635; Racelogic VBOX dual antenna (VB3i SL) 100-Hz GPS Data Logger. The testing maneuvers were performed at the airport Alkersleben, Germany. Straight-line braking maneuvers were done in high and low road friction conditions. Braking tests in low friction conditions were

TABLE II
Evaluation of the Developed WSCs

Evaluation metric	Control						
	RB	PI	PI RA	SMPI	SMPI RA	ISM	ISM RA
Low road friction conditions							
Median braking distance (m)	49.9	37.2	36.9	35.6	35.3	35.2	34.5
Max. braking distance (m)	54.4	37.5	37.7	35.9	35.9	36.0	35.7
Min. braking distance (m)	45.3	34.8	34.7	33.6	33.6	33.7	33.7
Wheel slip FL RMSD (-)	-	0.05	0.05	0.04	0.04	0.03	0.03
Wheel slip FR RMSD (-)	-	0.06	0.06	0.04	0.04	0.04	0.03
Wheel slip RL RMSD (-)	-	0.03	0.03	0.03	0.03	0.02	0.02
Wheel slip RR RMSD (-)	-	0.03	0.03	0.03	0.03	0.03	0.02
Deceleration STD (m/s^2)	0.11	0.06	0.05	0.06	0.05	0.06	0.05
High road friction conditions							
Median braking distance (m)	44.1	43.6	42.6	42.4	42.3	40.7	40.1
Max. braking distance (m)	44.5	44.7	43.9	43.3	43.1	41.1	40.2
Min. braking distance (m)	43.2	42.6	41.9	41.7	41.7	40.1	39.2
Wheel slip FL RMSD (-)	-	0.14	0.18	0.08	0.08	0.04	0.03
Wheel slip FR RMSD (-)	-	0.14	0.18	0.09	0.10	0.05	0.04
Wheel slip RL RMSD (-)	-	0.12	0.13	0.04	0.03	0.04	0.04
Wheel slip RR RMSD (-)	-	0.12	0.14	0.04	0.04	0.05	0.04
Deceleration STD (m/s^2)	0.11	0.12	0.11	0.11	0.11	0.08	0.08

done from initial velocity of 60 km/h due to limitations in the road section length, while 100 km/h was the initial velocity for high road friction conditions.

Represented WSC algorithms were tested in the closed loop with the state estimator, i.e., using only on-board sensors installed on the serial production vehicle. To evaluate advantages of developed controls over the state-of-the-art solutions, for comparison typical switching RB control was considered, which is characterized by deep periodic cycles of the wheel slip, especially for SUVs. To evaluate effectiveness of the RA algorithm, both cases with adaptive and preset reference wheel slip are considered. The preset value was selected to be so close as possible to the optimal area of the F_x-λ diagram.

After preliminary tuning of the control gains in simulation and on the brake hardware-in-the-loop test rig, they were adjusted on the vehicle during the tests in low road friction conditions. As soon as appropriate RMSD values of the wheel slip were achieved for each control strategy, six developed controller configurations were further considered and numerically evaluated in Table II: PI, SMPI, and ISM with the constant reference wheel slip, and with RA algorithm. Important to admit, that five test repetitions were considered for the evaluation of each control strategy. Compared to the switching RB control, on the low-friction road surface, the braking distance was reduced by application of developed controls with and without RA algorithm in 25% and 31%, respectively (see Fig. 12). The shortest stopping distance was achieved by the ISM RA control, which is on 7% and 2% shorter than PI RA and SM RA correspondingly. More robust operation of the system can be seen by comparing variations of the braking distance: switching RB causes deviation in 9% from the median value, while this can be reduced up to 3% in the case of the ISM RA control (see Fig. 12). Assessing the effectiveness of the RA algorithm itself, it provides

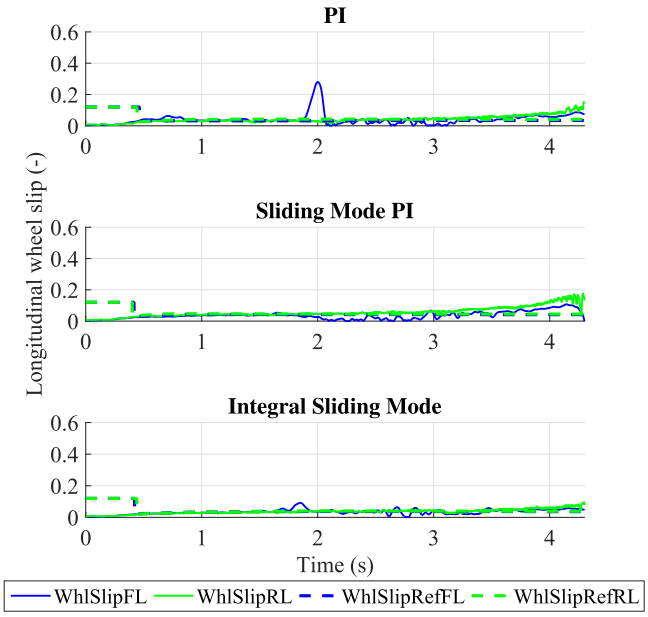

Fig. 9. WSC on the low-μ surface. PI, SMPI, and ISM controls with reference wheel slip adaptation.

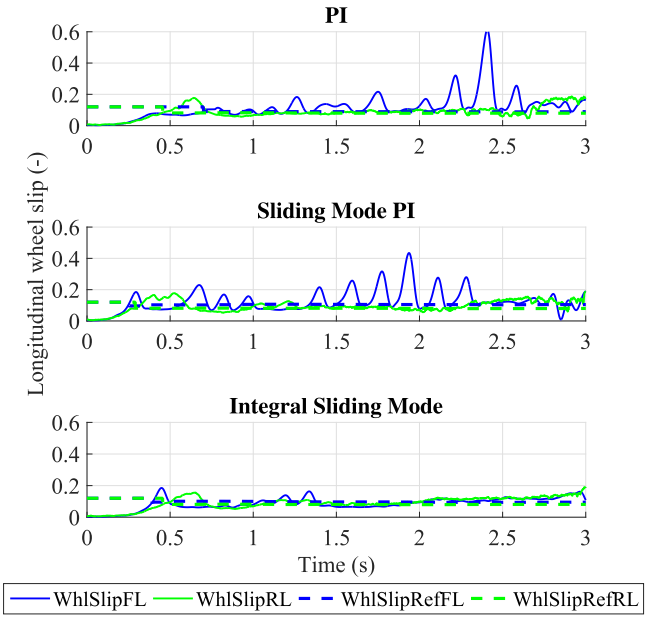

Fig. 10. WSC on the high-μ surface. PI, SMPI, and ISM controls with reference wheel slip adaptation.

a reduction in braking distance up to 2% in comparison to the cases with the preset reference wheel slip. It confirms hypothesis that during the emergency braking, the optimal area of the F_x–λ diagram can deviate from its initial value and emphasizes importance of the RA. In particular, the reference wheel slip in low-μ conditions varied during the test in the range from 0.02 up to 0.05, while preset reference value was at 0.04. All six controller types have evident advantage over the switching RB control in terms of ride quality by reducing longitudinal deceleration oscillations in 55% as indicated by STD of the deceleration in Table II. This is achieved by smooth tracking of the wheel slip as well as by the proper estimation of the reference wheel slip and its slow variation; see Fig. 9.

Existing continuous WSC methods do not assure required robustness. Once the control gains are properly tuned for the low-μ road surface, the control can produce more oscillatory behavior in high-μ friction conditions that is caused by the nature of tire–road interaction. Therefore, to check the robustness, control gains were kept the same as during the tests on the low-μ surface. As a result, wheel slip RMSD remained at almost the same level for SMPI and ISM, while PI control has three-four times higher deviations due to the more oscillatory behavior; see Fig. 10. In terms of the braking distance and ride quality, it leads in the case of PI control with constant wheel slip reference ($\lambda^* = 0.1$) to comparable results with the switching RB control. Even by applying PI RA, a 3% shorter braking distance can be attained with still comparable ride quality. Moreover, difference between the minimal and maximal braking distance remains in a quite high range for the PI control (see Fig. 12) that indicates insufficient robustness. A similar problem occurs with SMPI control, which produces more chattering on the high-μ road (see Fig. 11). It results in almost the same ride quality, while the

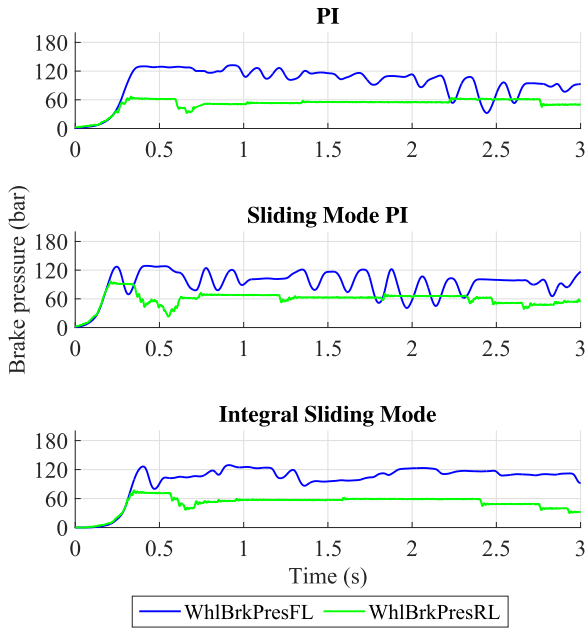

Fig. 11. WSC on the high-μ surface. Brake pressure oscillations of the PI and SMPI controls lead to significant reduction of the braking force and increased longitudinal vehicle jerk.

braking distance is reduced in 4% compared to the switching RB control. Much better results were shown by the ISM, where the braking distance was reduced on 9% and ride quality was improved on 27%. Important to admit that by application of the RA strategy, less effect in reduction of the braking distance in high road friction conditions was attained. It happens due to the

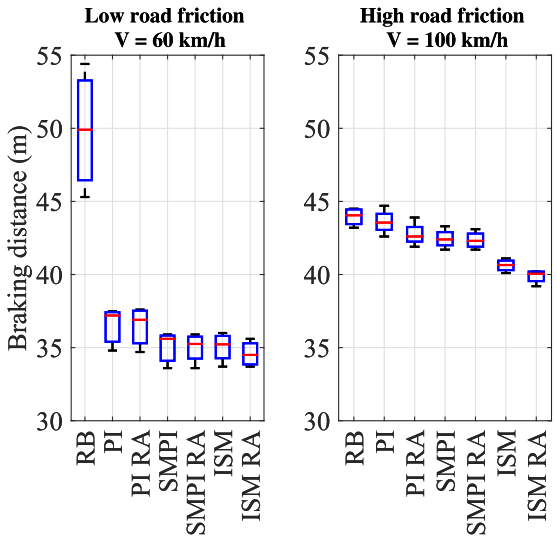

Fig. 12. Vehicle braking distance on the low- and high-μ surfaces for different configurations of the WSC.

thinner optimal area of F_x–λ diagram and a more homogeneous type of the road surface, where variation of the reference wheel slip produced by RA was from 0.09 up to 0.11 remaining most of the time at 0.1.

VI. Conclusion

The performed study allows formulating several conclusions, essential for designing and control of the decoupled brake system intended to be used both on conventional vehicles and on EVs.

1) The continuous WSC, based on PI, SMPI, and ISM control, can give significant benefits in the braking distance reduction (up to 31%) and reduction of longitudinal deceleration oscillations up to 55% on the low-μ road surface.
2) Due to the insufficient robustness of PI and chattering of SMPI controls, on the high-μ road surface only ISM control can simultaneously produce the braking distance reduction up to 9% and improved ride quality up to 27% through smooth and precise wheel slip tracking.
3) RA logic is necessary element of the WSC, which can reduce braking distance on additional 2% compared to the control with the reference wheel slip preset close to the optimal area. RA should be tuned adjusted to avoid the risk of control quality deterioration. This adjustment can be done by evaluating the RMSD of the wheel slip.

Following future activities are planned to be done considering obtained results and performed analysis.

1) Observer of the effective tire radius is planned for the implementation to the state and parameter estimator to provide a precise wheel slip estimation also for the tires with higher profile.
2) Developed WSC will be integrated with the novel active tire pressure control system to provide even shorter braking distance [29].

Appendix A
Experimental Validation of the State and Parameter Estimator

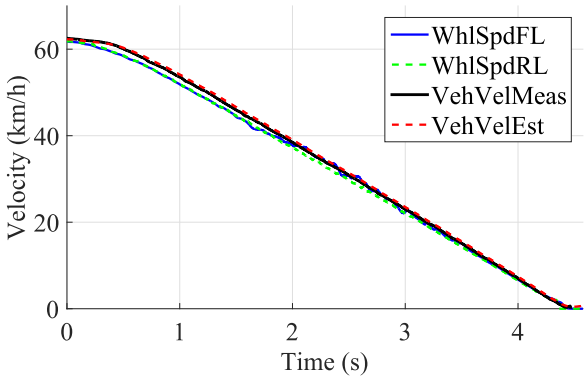

Fig. 13. Validation of the longitudinal vehicle velocity observer O_{V_x}. The reference measurements were obtained over GPS by VBOX.

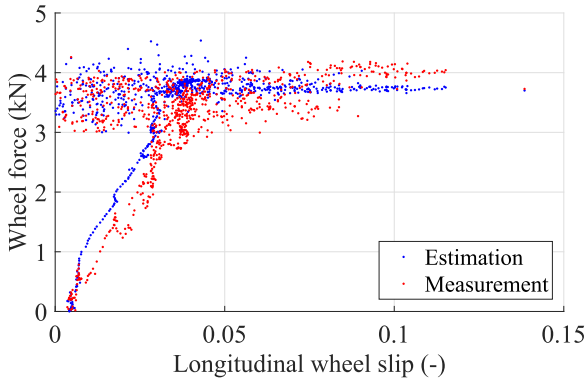

Fig. 14. Validation of the longitudinal wheel force observer O_{F_x}. The measuring wheel hub was mounted at the front right wheel.

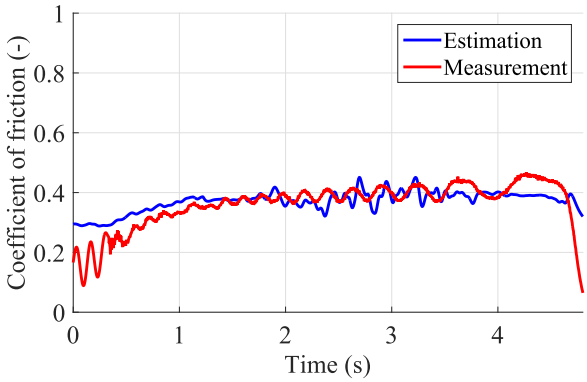

Fig. 15. Validation of the brake lining coefficient of the friction observer O_{μ_l}. Measured value was obtained using information from the measuring hub and pressure sensor mounted close to the caliper.

APPENDIX B
VEHICLE SPECIFICATIONS

TABLE III
VEHICLE TECHNICAL DATA

Vehicle	
Vehicle type	Land Rover Range Rover Evoque
Full mass (kg)	2275
Driveline	Front wheel drive
Maximal speed (km/h)	182
Tire size	235/55 R19
Wheelbase (m)	2.660
Track width (m)	1.625
Drag coefficient	0.35
Frontal surface (m^2)	2.323
Gearbox	Six-speed, manual
Engine type	Diesel internal combustion engine
Engine capacity (l)	1.999
Maximal engine power (kW)	110
Maximal engine power (Nm)	380
Brakes	
Front equivalent brake radius (m)	0.12
Rear equivalent brake radius (m)	0.1325
Front brake cylinder diameter (m)	0.057
Rear brake cylinder diameter (m)	0.04

ACKNOWLEDGMENT

The authors would like to thank T. Pütz (ZF TRW), F. Brungs (ZF TRW), R. Sutton (Southtown Engineering), P. Barber (Jaguar Land Rover), and R. Boyd (Jaguar Land Rover) for their support in reinstrumentation of the vehicle demonstrator.

REFERENCES

[1] S. Murata, "Innovation by in-wheel-motor drive unit," *Veh. Syst. Dyn.*, vol. 50, no. 6, pp. 807–830, 2012.
[2] H. Fujimoto and K. Maeda, "Optimal yaw-rate control for electric vehicles with active front-rear steering and four-wheel driving-braking force distribution," in *Proc. 39th Annu. Conf. IEEE Ind. Electron. Soc.*, 2013, pp. 6514–6519.
[3] Y. Wang, H. Fujimoto, and S. Hara, "Driving force distribution and control for EV with four in-wheel motors: A case study of acceleration on split-friction surfaces," *IEEE Trans. Ind. Electron.*, vol. 64, no. 4, pp. 3380–3388, Apr. 2017, doi: 10.1109/TIE.2016.2613838.
[4] H. Gao, X. Zhang, Y. Liu, and D. Li, "Longitudinal control for Mengshi autonomous vehicle via Gauss cloud model," *Sustainability*, vol. 9, no. 12, p. 2259, 2017.
[5] G. Xie, H. Gao, L. Qian, B. Huang, K. Li, and J. Wang, "Vehicle trajectory prediction by integrating physics-and maneuver-based approaches using interactive multiple models," *IEEE Trans. Ind. Electron.*, vol. 65, no. 7, pp. 5999–6008, Jul. 2017.
[6] H. Jing, Z. Liu, and H. Chen, "A switched control strategy for antilock braking system with on/off valves," *IEEE Trans. Veh. Technol.*, vol. 60, no. 4, pp. 1470–1484, May 2011.
[7] J. J. Castillo, J. A. Cabrera, A. J. Guerra, and A. Simón, "A novel electrohydraulic brake system with tire–road friction estimation and continuous brake pressure control," *IEEE Trans. Ind. Electron.*, vol. 63, no. 3, pp. 1863–1875, Mar. 2016.
[8] D. Savitski, V. Ivanov, K. Augsburg, B. Shyrokau, R. Wragge-Morley, T. Pütz, and P. Barber, "The new paradigm of an anti-lock braking system for a full electric vehicle: Experimental investigation and benchmarking," *Proc. Inst. Mech. Eng., D, J. Automobile Eng.*, vol. 230, no. 10, pp. 1364–1377, 2016.
[9] D. Savitski, V. Ivanov, B. Shyrokau, J. D. Smet, and J. Theunissen, "Experimental study on continuous ABS operation in pure regenerative mode for full electric vehicle," *SAE Int. J. Passenger Cars-Mech. Syst.*, vol. 8, no. 2015-01-9109, pp. 364–369, 2015.
[10] S. Drakunov, U. Ozguner, P. Dix, and B. Ashrafi, "ABS control using optimum search via sliding modes," *IEEE Trans. Control Syst. Technol.*, vol. 3, no. 1, pp. 79–85, Mar. 1995.
[11] M. Amodeo, A. Ferrara, R. Terzaghi, and C. Vecchio, "Wheel slip control via second-order sliding-mode generation," *IEEE Trans. Intell. Transp. Syst.*, vol. 11, no. 1, pp. 122–131, Mar. 2010, doi: 10.1109/TITS.2009.2035438.
[12] Y. W. Liang, C. C. Chen, D. C. Liaw, and Y. T. Wei, "Nonlinear reliable control with application to a vehicle antilock brake system," *IEEE Trans. Ind. Informat.*, vol. 9, no. 4, pp. 2114–2123, Nov. 2013, doi: 10.1109/TII.2012.2234470.
[13] R. de Castro, R. E. Araùjo, and D. Freitas, "Wheel slip control of EVs based on sliding mode technique with conditional integrators," *IEEE Trans. Ind. Electron.*, vol. 60, no. 8, pp. 3256–3271, Aug. 2013, doi: 10.1109/TIE.2012.2202357.
[14] T. Shim, S. Chang, and S. Lee, "Investigation of sliding-surface design on the performance of sliding mode controller in antilock braking systems," *IEEE Trans. Veh. Technol.*, vol. 57, no. 2, pp. 747–759, Mar. 2008, doi: 10.1109/TVT.2007.905391.
[15] M. Tanelli and A. Ferrara, "Enhancing robustness and performance via switched second order sliding mode control," *IEEE Trans. Automat. Control*, vol. 58, no. 4, pp. 962–974, Apr. 2013, doi: 10.1109/TAC.2012.2225553.
[16] E. Kayacan, Y. Oniz, and O. Kaynak, "A grey system modeling approach for sliding-mode control of antilock braking system," *IEEE Trans. Ind. Electron.*, vol. 56, no. 8, pp. 3244–3252, Aug. 2009, doi: 10.1109/TIE.2009.2023098.
[17] K. Berntorp, "Joint wheel-slip and vehicle-motion estimation based on inertial, GPS, and wheel-speed sensors," *IEEE Trans. Control Syst. Technol.*, vol. 24, no. 3, pp. 1020–1027, May. 2016, doi: 10.1109/TCST.2015.2470636.
[18] W. Y. Wang, I. H. Li, M. C. Chen, S. F. Su, and S. B. Hsu, "Dynamic slip-ratio estimation and control of antilock braking systems using an observer-based direct adaptive fuzzy-neural controller," *IEEE Trans. Ind. Electron.*, vol. 56, no. 5, pp. 1746–1756, May. 2009, doi: 10.1109/TIE.2008.2009439.
[19] D. Nesic, A. Mohammadi, and C. Manzie, "A framework for extremum seeking control of systems with parameter uncertainties," *IEEE Trans. Automat. Control*, vol. 58, no. 2, pp. 435–448, Feb. 2013, doi: 10.1109/TAC.2012.2215270.
[20] C. Lee, K. Hedrick, and K. Yi, "Real-time slip-based estimation of maximum tire-road friction coefficient," *IEEE/ASME Trans. Mechatronics*, vol. 9, no. 2, pp. 454–458, Jun. 2004, doi: 10.1109/TMECH.2004.828622.
[21] S. Semmler, "Regelung der Fahrzeugbremsdynamik mit kontinuierlich einstellbaren Radbremsen," *Fortschritt Berichte-VDI Reihe 12 Verkehrstechnik Fahrzeugtechnik*, vol. 632, pp. 63–68, 2006.
[22] Z. Qi, S. Taheri, B. Wang, and H. Yu, "Estimation of the tyre-road maximum friction coefficient and slip slope based on a novel tyre model," *Vehicle Syst. Dyn.*, vol. 53, no. 4, pp. 506–525, 2015, doi: 10.1080/00423114.2014.1002795. [Online]. Available: http://dx.doi.org/10.1080/00423114.2014.1002795
[23] B. Ganzel, "Slip control boost braking system," US Patent 9 221 443, Dec. 29, 2015.
[24] R. Rajamani, G. Phanomchoeng, D. Piyabongkarn, and J. Y. Lew, "Algorithms for real-time estimation of individual wheel tire-road friction coefficients," *IEEE/ASME Trans. Mechatronics*, vol. 17, no. 6, pp. 1183–1195, Dec. 2012, doi: 10.1109/TMECH.2011.2159240.
[25] S. M. Savaresi and M. Tanelli, *Active Braking Control Systems Design for Vehicles*. London, U.K.: Springer, 2010.
[26] V. I. Utkin, *Sliding Modes in Control and Optimization*. Berlin, Germany: Springer, 2013.
[27] V. Utkin and J. Shi, "Integral sliding mode in systems operating under uncertainty conditions," in *Proc. IEEE 35th Conf. Decision Control*, 1996, vol. 4, pp. 4591–4596.
[28] M. Tanelli, L. Piroddi, and S. M. Savaresi, "Real-time identification of tire–road friction conditions," *IET Control Theory Appl.*, vol. 3, no. 7, pp. 891–906, 2009.
[29] D. Savitski, K. Hoepping, V. Ivanov, and K. Augsburg, "Influence of the tire inflation pressure variation on braking efficiency and driving comfort of full electric vehicle with continuous anti-lock braking system," *SAE Int. J. Passenger Cars-Mech. Syst.*, vol. 8, no. 2015-01-0643, pp. 460–467, 2015.

Dzmitry Savitski (S'12–M'18) was born in Minsk, Belarus, on December 27, 1987. He received the Dipl.-Ing. degree in automotive engineering from Belarusian National Technical University, Minsk, in 2011. From 2011 to 2018, he was working toward the Dr.-Ing. degree in automotive engineering with Technische Universität Ilmenau, Ilmenau, Germany.

From 2009 to 2011, he was a Research Assistant with the Division for Computer Vehicle Design, Joint Institute of Mechanical Engineering, Minsk. He is currently a Research Fellow with Automotive Engineering Group, Technische Universität Ilmenau. His current research interests include vehicle dynamics control, chassis systems design and control, and terramechanics.

Dr. Savitski is a Member of the Association of German Engineers, the Society of Automotive Engineers, and the Tire Society.

Dmitrij Schleinin received the B.Sc. degree in mechanical engineering and the M.Sc. degree in automotive engineering from Technische Universität Ilmenau, Ilmenau, Germany, in 2014 and 2016, respectively.

He was a Research Fellow with Automotive Engineering Group, Technische Universität Ilmenau, until 2018. Since 2018, he joined dSPACE GmbH, Ingolstadt, Germany, as the Application Engineer. His research interests include vehicle dynamics control, automated driving, and advanced driver assistance systems. Mr. Schleinin is a Member of the Association of German Engineers

Valentin Ivanov (M'13–SM'15) received the Ph.D. and D.Sc. degrees in automotive engineering from Belarusian National Technical University, Minsk, Belarus, in 1997 and 2006, respectively, and the Dr.-Ing. habil. degree in automotive engineering from Technische Universität Ilmenau, Ilmenau, Germany, in 2017.

From 1995 to 2007, he was consequently an Assistant Professor, an Associated Professor, and a Full Professor with the Department of Automotive Engineering, Belarusian National Technical University. In July 2007, he became an Alexander von Humboldt Fellow, and in July 2008, he became a Marie Curie Fellow with Technische Universität Ilmenau. He is currently EU Project Coordinator with the Automotive Engineering Group, Technische Universität Ilmenau. His research interests include vehicle dynamics, electric vehicles, automotive control systems, chassis design, and fuzzy logic.

Prof. Ivanov is a member of the SAE International, the Society of Automotive Engineers of Japan, the Association of German Engineers, IFAC (Technical Committee "Automotive Control"), and the International Society for Terrain-Vehicle Systems.

Klaus Augsburg received Dr.-Ing. degree in automotive engineering from Technische Universität Dresden, Germany, in 1985.

From 1984 to 1993, he worked in industry on leading engineer positions, and then, as a Senior Research Assistant with Technische Universität Dresden, Dresden, Germany, in 1993–1999. In 1999, he became a Full Professor and the Chair of the Automotive Engineering Group, Technische Universität Ilmenau, Ilmenau, Germany. He is also the Chairman of Workgroup Automotive Engineering VDI Thüringen and the Chief Executive Officer of Steinbeis-Transferzentrum Fahrzeugtechnik. He founded Thuringian Centre of Innovation in Mobility in 2011, where he is coordinating public research projects and bilateral projects with industrial partners. He is author of more than 100 research papers, guest lectures, and patents.

Prof. Augsburg is a Member of the Association of German Engineers.